THE INVESTIGATIONS OF MULTI-LAYER INTERFACE FAILURE BEHAVIOR FOR SISAL FIBER REINFORCED COMPOSITES VIA ACOUSTIC EMISSION AND FINITE ELEMENT METHOD

Qian Li[1], Yan Li[*2] and Limin Zhou[3]

[1, 2] School of Aerospace Engineering and Applied Mechanics, Tongji University, 1239 Siping Road, Shanghai, P.R. China
[2] Key Laboratory of Advanced Civil Engineering Materials, Ministry of Education, Tongji University, 1239 Siping Road, Shanghai, P.R. China
[1, 3] Department of Mechanical Engineering, The Hong Kong Polytechnic University, Hong Kong, P.R. China
[1]Email: 1310541@tongji.edu.cn
[2]Email: liyan@tongji.edu.cn
[3]Email: li.min.zhou@polyu.edu.hk

Keywords: Plant fibers, Interface, Multi-layer, Acoustic emission, Finite element analysis

ABSTRACT

The mechanical performances of composite materials are largely dependent on their interfacial properties in composite structure design. The interfacial failure behaviors of sisal fiber reinforced composites (SFRCs) were investigated experimentally and theoretically in present study. Single fiber pull-out experiments were performed on sisal fibers with the multi-layer structure. To gain insight into the multi-layer interfacial failure mechanisms of SFRCs, acoustic emission (AE) technique was employed on monitoring and characterizing the multi-stage fracture performance observed in the pullout process. The energy emission for multi-stage fracture of SFRC was observed to gradually reduce due to their decreased residual pullout strength. Different failure sequences of SFRCs were described with the help of AE. Based on the above results, statistical analysis was used to evaluate the probability of technical fiber, elementary fiber and microfibril pullout. The results indicated that technical fiber was more likely to be pulled-out from matrix since the interfacial bonding between sisal fiber and matrix was relatively poor for untreated sisal fiber while elementary fiber and microfibril could also be pulled-out from technical fiber owing to the existence of the multi-layer interface. Meanwhile, based on the traditional shear lag model, a three-interface finite element model, regarding multi-stage fracture of the three interfaces, was established to interpret the multi-layer failure phenomenon and estimate the stress variation of SFRCs during the single sisal fiber pull-out process. Quantitative comparison between the numerical simulation of three-interface model and that of single and double interface models, using the experimental applied stress as reference, surmised that single, double and three-interface model need to be comprehensively considered to describe the pullout behaviors of SFRCs for providing more accurate solutions. It was shown that a good agreement was obtained by comparing numerical modelling results with experimental ones in the single fiber pull-out tests.

1 INTRODUCTION

The past decades have witnessed that plant fibers used as reinforcing materials for green composites have gained ground for sporting goods, automotive and aerospace fields due to their abundant source, competitive price, promising specific mechanical properties (e.g., tensile strength, modulus and fracture elongation) [1, 2], superior environmental performance (e.g., recyclability and biodegradability) [3, 4] and superior functional properties (e.g., sound absorption, thermal insulation and damping properties) [5, 6]. Plant fiber reinforced composites (PFRCs) have become the ideal and promising alternatives to traditional synthetic fiber reinforced composites for the future applications. However, the distinct multi-layer and multi-scale structure of plant fibers relative to synthetic fibers could lead to different interfacial mechanical performance and failure modes. Rare reported work was

found to comprehensively explore the multi-layer interfacial properties of PFRCs and illustrate the influence of the multi-layer structure of plant fibers on their interfacial failure behaviors.

Experience has verified that the interfacial performances of the composite materials play a much more decisive role in their overall mechanical properties [7-10]. The interfacial performances of the composites have been experimentally characterized and evaluated by developing varied micromechanical techniques, including single fiber pull-out [11], push-out [12], fragment [13] and micro-droplet [14] measurement. Among them, single fiber pull-out measurement is one prevailing method to analyze the interfacial debond process and determine interfacial stress distributions. During a typical pull-out process of synthetic fiber reinforced composites (i.e., carbon fiber reinforced composites (CFRCs) or glass fiber reinforced composites (GFRCs)) [15-18], the applied stress firstly increases linearly with the increase of the displacement until debonding initiates, followed by a significant drop in the applied stress due to complete debonding of the interface between the fiber and matrix. Consequently, only the interfacial performances between the fiber and matrix can be considered for CFRCs or GFRCs with uniform and homogeneous microstructure. To comprehensively evaluate the fiber pull-out behavior of synthetic fiber reinforced composites, a rich body of literature recapitulating theoretical modeling of debonding behavior of fiber/matrix interface for CFRCs or GFRCs has been reported [19-21]. Representatively, relying on the fracture mechanics, their interfacial properties (i.e., interfacial strength, fracture toughness, frictional coefficient) can be calculated through combining the curve result of the pull-out experiment and the relevant theoretical model. Zhou et al. [19, 20] presented a theoretical model to describe the interfacial debonding and fiber pull-out behaviors of CFRCs. The theoretical analysis achieved a good agreement with experimental data. Liu et al. [21] developed a fiber sliding model to study the effects of the rough interface and residual clamping stress on the frictional pull-out stress of single CFRCs, ending up with the interesting results. Subsequently, some simulation studies have been conducted to demonstrate the whole fiber pull-out process [22-24]. In addition, few studies have been reported to reveal the crack propagation mechanisms of the macro composite laminates and validate their relevant failure modes by employing the acoustic emission method [25, 26]. However, plant fibers possess complex multi-layer cell wall and lumen structures [4, 27]. Their cell walls are reinforced with helical microfibrillar bands of cellulose in a hemi-cellulose and lignocellulosic matrix. Meanwhile, single plant fibers can be considered as a kind of composite consisting of some elementary fibers bonded by pectin matrix. Thus, the unique and complex multi-scale and multi-layer failure behaviors can be obviously observed in plant fibers and their reinforcing composites [25, 28, 29]. Rare research work mentioned the relationship between the hierarchical structure of plant fibers and the interfacial mechanical properties of PFRCs and developed the finite element model with the multi-layer interface.

To facilitate the comprehending of this relationship, the current study was organized in the order of experimental interpretation and theoretical validation. The multiple interfacial debonding behaviors of sisal fiber reinforced composites (SFRCs) were investigated by both experimental and theoretical characterization in the present study. Statistical analysis was used to evaluate the probability of multiple debond and pullout. The failure process of the pulled-out sisal fibers was monitored and characterized with AE technique. Time frequency analysis on the original AE signals were comparably conducted by using Hilbert-Huang transform (HHT). The failure modes in single sisal fiber pull-out tests were observed with the aid of Scanning Electronic Microscopy (SEM). Finally, based on the traditional shear lag model, a three-interface finite element model, regarding multi-stage fracture of the three interfaces, was established to interpret the multi-layer failure phenomenon and estimate the stress variation of SFRCs during the single sisal fiber pull-out process.

2 MATERIALS AND EXPERIMENTS

Sisal fibers with a density of 1.45 g/cm^3 supplied by Guangxi Sisal Group Co., Ltd, epoxy resin (NPEL-128), curing agent (EH-6303) and accelerator (EH-6412) purchased by Shanghai Zhongsi Industry Co., Ltd were used for sample preparation for the single fiber pull-out experiment in the

present study. Matrix was formulated of epoxy resin (100 wt. %), curing agent (26 wt. %) and accelerator (8 wt. %) and the mixture featured a volume density of 1.2 g/cm^3.

First, treated sisal fibers and mixed epoxy matrix were used to prepare specimen for single fiber pull-out experiment. The specimen preparations for the single fiber pull-out experiments were conducted through the following procedures [23, 24]: Firstly, the sisal fibers were pretreated by washing in deionized water at 70 $°C$ for 1 h to remove impurities, hackling and arraying for straightening and drying in a vacuum oven at 105 $°C$ for 2 h to remove the absorbed moisture. Secondly, 200 dried fibers, of which diameters were measured via an optical microscopy (OM, 10XB-PC, China) at 100 times magnification, were randomly selected (to obtain different fiber fracture modes) and chopped into short fibers with a length of 20 mm. The diameters of sisal fibers were statistically assessed using the analysis of the Weibull distribution. Thirdly, the prepared sisal fibers were separately stuck into a cylindrical silicon rubber mold with a dimension of 20 mm (diameter) × 20 mm (height) using a sewing needle. The embedded fiber length ranged from 100 to 500 μm. Next, the mixed epoxy resin was meticulously poured into the mold after being evacuated in the vacuum oven for 10 minutes to eliminate air bubbles and then cured in the mold at room temperature for 24 h. Finally, the specimens were carefully taken out from the molds and fully post-cured at 60 $°C$ for 2 h.

After the specimens were well prepared, the single sisal fiber pull-out experiments were carried out on a universal mechanical testing machine (Wance, Shenzhen, China) with a gauge length of 10 mm at a crosshead speed of 0.5 mm/min. The applied force and the displacement were recorded. Then, acoustic emission (AE) monitoring was simultaneously performed in the single sisal fiber pull-out tests by applying a SAEU2S system (Soundwel Technology Co., Ltd, Beijing, China), of which test strategy and mechanism were presented in Figure 1. AE measurements were conducted by employing single SR150M sensor with a resonant frequency range of 20 to 400 kHz and a preamplifier (35 dB) with a bandwidth of 10 kHz to 2 MHz. The threshold was set as 35 dB to exclude the majority signals of background noises.

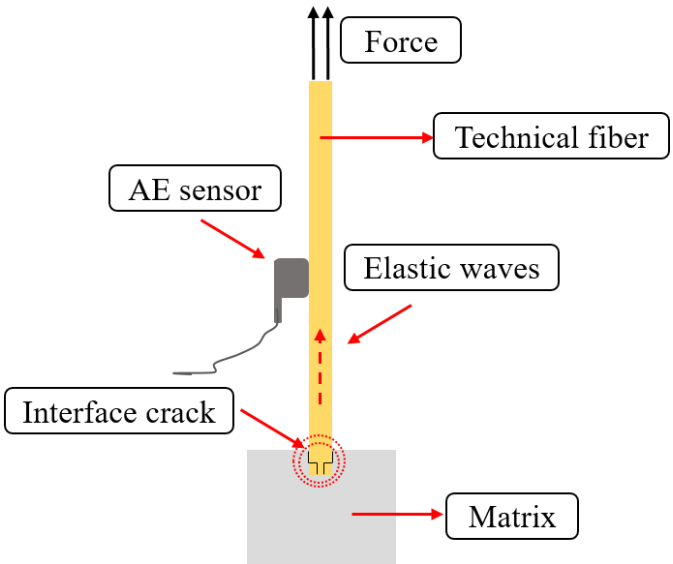

Figure 1: Schematic illustration of the mechanism of acoustic emission measurement for the single sisal fiber pull-out tests.

Finally, after the pull-out tests, the debond lengths of the fibers were measured with the aid of OM. And a field emission SEM (FE-SEM, XL30 FEG, PHILIPS Co., Netherlands) was employed to observe the surface morphology and microstructures and failure modes of the pulled-out sisal fibers.

3 THEORETICAL ANALYSIS

The finite element method (FEM) is used for simulating the process of multi-stage pullout measurements and obtaining the stress distributions in whole pull-out procedure via the commercial finite element software ABAQUS.

A double interface theoretical model for single plant fiber pull-out tests has been developed in our earlier researches and discussion on the basis of existing shear lag model, Coulomb friction law, fracture mechanics concept and Griffith energy balance equation [10]. A technical fiber that consists of several elementary fibers is embedded in the center of the coaxial matrix and a tensile stress is applied to the top end of the embedded fiber. Two types of interfacial failure modes occurred in single plant fiber pull-out test, named as process 1 and process 2. In process 1, the interfacial debonding between technical fiber and matrix starts, and the following debonding occurs between elementary fibers as shown in process 2. The interfacial debonding criterions and the solutions for the axial stresses distributions, the partial debond stresses, the maximum debond stresses, the external applied stresses and the initial frictional pull-out stresses in the pull-out processes of plant fiber reinforced composites are obtained and the detailed theoretical analysis and calculation procedures could refer to our previous paper [10].

In current study, three-interface models were established based on the experimental phenomenon of single sisal fiber pullout tests. The basic parameters for numerical simulation are listed in Table 1 according to our previous work [3]. The illustration of the finite element model is shown in Figure 2 (a). To simplify the calculation process, one quarter model with mesh is employed on the specific analysis in present study as displayed in Figure 2 (b). And the cohesive element is used to simulate the multi-layer interfaces of SFRCs.

	Properties of Fiber			Properties of Matrix		
Type	Fiber Type		Sisal	Matrix Type		Epoxy
Young's Modulus	E_{f1}	$[GPa]$	10.06	E_m	$[GPa]$	3
Poisson's Ratio	n_{f1}	/	0.12	n_m	/	0.16
Radius	a_1	$[mm]$	0.093			
	a_2	$[mm]$	0.065	b	$[mm]$	10
	a_3	$[mm]$	0.034			
Thermal Expansion Coefficient	α_{f1}	$[10^{-6}/°C]$	10.8	α_m	$[10^{-6}/°C]$	70.8
				Interfacial Properties		
Interface Type			Sisal/Epoxy	Between elementary fibers		Between cell walls
Embedded Fiber Length L	$[mm]$			0.1~0.5		
Coefficient of Friction m_1, m_2, m_3	/		4.42	1.12		1.02
Temperature Change ΔT	$[°C]$			-100		
Fracture Toughness $G_{ic1}, G_{ic2}, G_{ic3}$	$[J/m^2]$		133	18.1		12.4

Table 1: Material properties and geometric factors.

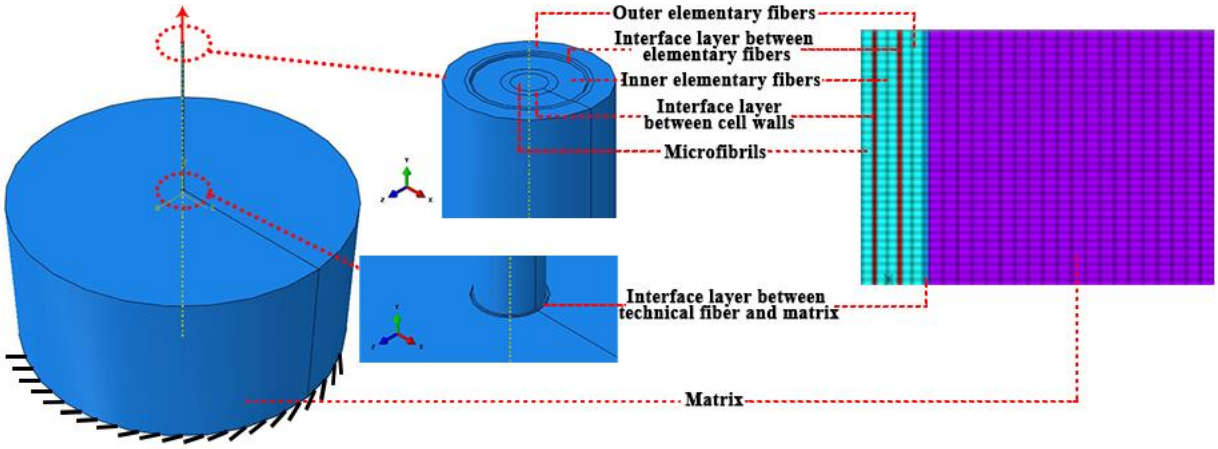

(a)

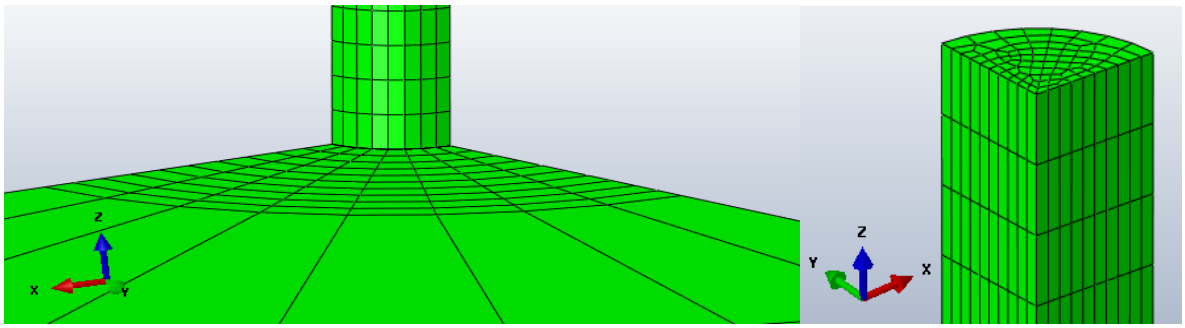

(b)

Figure 2: Finite element model of the single sisal fiber pull-out with multi-layer interfaces: (a) original model and (b) one quarter model with mesh

4 RESULTS AND DISCUSSION

4.1 Single fiber pull-out behaviors of SFRCs monitored by AE technique

A series of plots were generated for acoustic emission (AE) events to evaluate the possible correlations with the failure behavior of SFRCs following multi-stage fracture (Figure 3). Figure 4 shows the AE energy behaviors of SFRCs during the pullout process. Variations in AE event energy reflected different damage mechanisms. There were two energy ranges of AE events for SFRCs, breakage of sisal technical fiber, elementary fiber and microfibrils at higher energies, fiber pulling-out at lower energies. It can be seen from Figure 4 (a) that the SFRCs with the single stage fracture had only one higher AE energy and following few lower energies during loading, which meant the whole sisal technical fiber broke and were pulled-out. Similarly, it can be also found in Figure 4 (b) and (c) that the SFRCs with the double and triple stage fracture had two and three higher AE energies emission events before the pullout process, respectively, suggesting that all elementary fibers broke at different time and the breakage of the microfibrils in cell wall layer occurred.

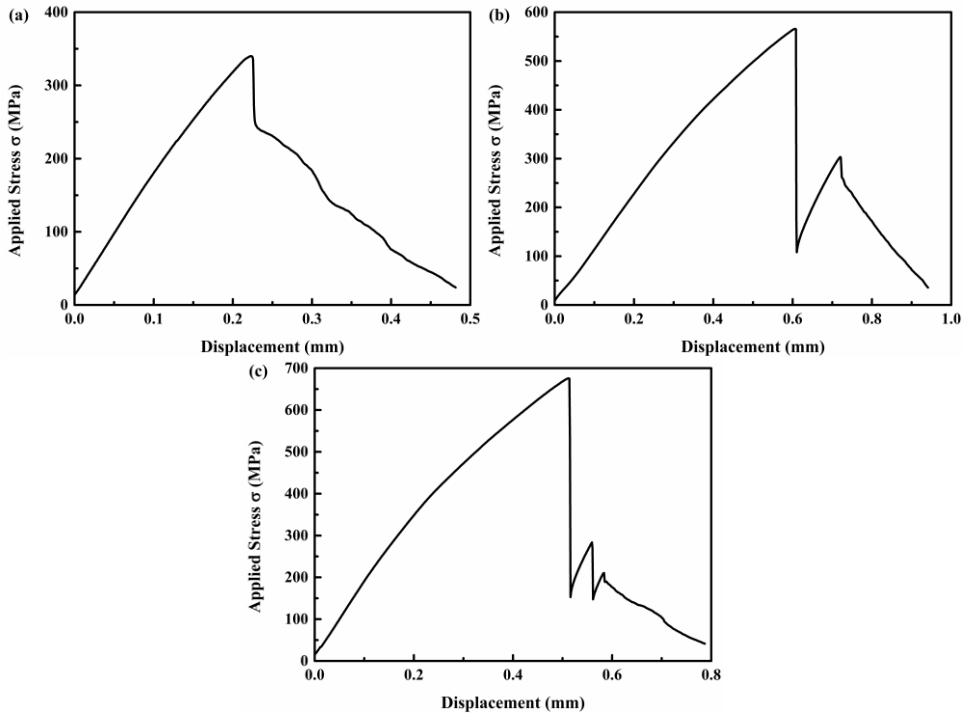

Figure 3: The applied stress-displacement curves of the single sisal fiber pull-out with (a) single, (b) double and (c) triple stage fracture.

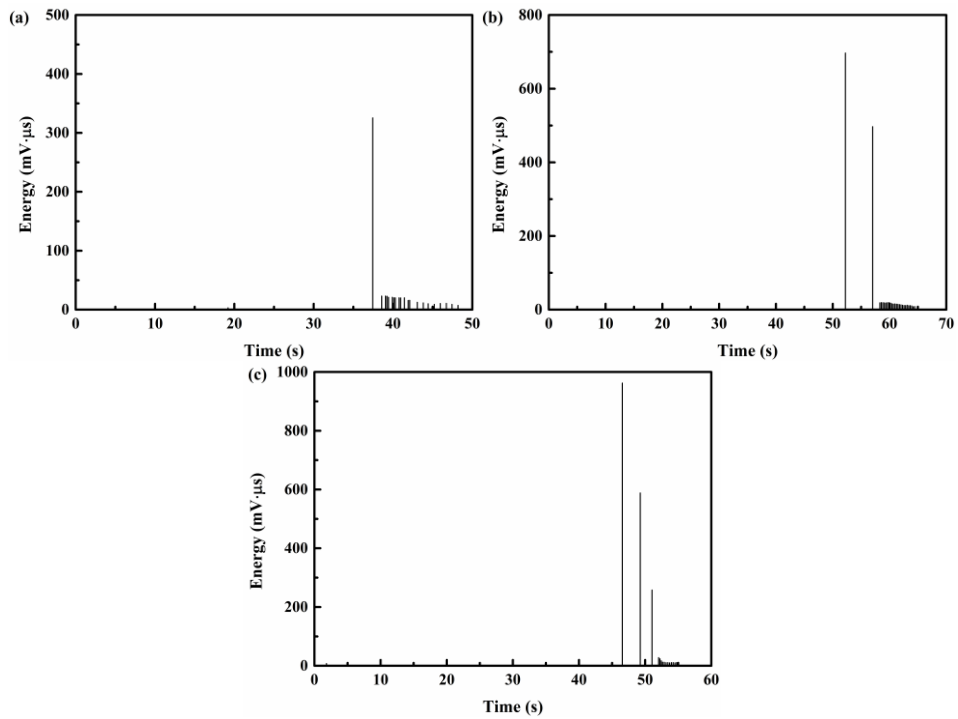

Figure 4: The acoustic emission response about energy versus time for the single sisal fiber pull-out with (a) single, (b) double and (c) triple stage fracture.

Previous research has illustrated that the generation of AE signals is physically linked to the asperities at the interface and the interfacial bonding status. From the theoretical derivation [30], amplitude (energy)-based and frequency-based analyses are predicted capable of characterizing AE signals generated at multi-layer interfaces with various asperities (i.e., IF-FM, IF-ELE and IF-CW interfaces) and further indicating the debonding process of the interfaces. In particular, the intrinsic

mode functions (IMFs) of AE signals, extracted from signals using an empirical mode decomposition (EMD), are used to characterize the debonding process (e.g., debonding and sliding friction) in the multi-layer interfaces of SFRCs undergone tensile stress, whereby to evaluate the debonding condition of the composites quantitatively. Specifically, the multi-stage debonding and sliding friction-related IMFs, generated in the single fiber pull-out measurements are ascertained via a Hilbert-Huang transform (HHT). Three types of pull-out failure behaviors, namely single-stage, double-stage and three-stage, are comparably used to exhibit the dependence of Wave energy attenuation (WED)-based method on the interface configurations.

The original AE signals (the average of 300 signals) generated at the multi-stage debonding interfaces (i.e., IF-FM, IF-ELE and IF-CW) are processed with HHT and their first decomposed IMFs are displayed in Figure 5 and comparably studied to ascertain their distinct characteristics. To investigate energy shift in the signals generated from the interface debonding under different process, the corresponding HHT spectra of the signals (first four IMFs) are comparably displayed in Figure 6. In addition, the main energy of the AE signal is observed to distribute in the frequency range between 20 and 200 kHz. Noted that S_i^T denotes the ith IMF of the AE signals generated from specimens under a process of T ($T = 11,\ 21,\ 22,\ 31,\ 32\ or\ 33$). From the comparison regarding signal envelopes in the time domain, a high similarity can be found between the original signal and its first IMF, which means the first IMF dominates the energy of the original signal. The HHT spectra presented with normalized energy of the four decomposed signals in Figure 5 (a)-(f) are comparatively shown in Figure 6 (a)-(f). The energy ratio of low-frequency components (below 25 kHz) becomes larger with the increase of debonded interface. Comparing the AE signals generated from the IF-FM debonding failure to those generated from the IF-ELE and IF-CW debonding failure, it is found that the IF-FM debonding failure generates the AE signals dominating the frequency range between 10 and 40 kHz, while the AE signals induced by the IF-ELE and IF-CW debonding failure mainly distribute between 20 and 200 kHz and between 30 and 220 kHz, respectively. The difference in roughness and hardness of those three interfaces (IF-FM, IF-ELE and IF-CW) is responsible for the diversity of their frequency distribution.

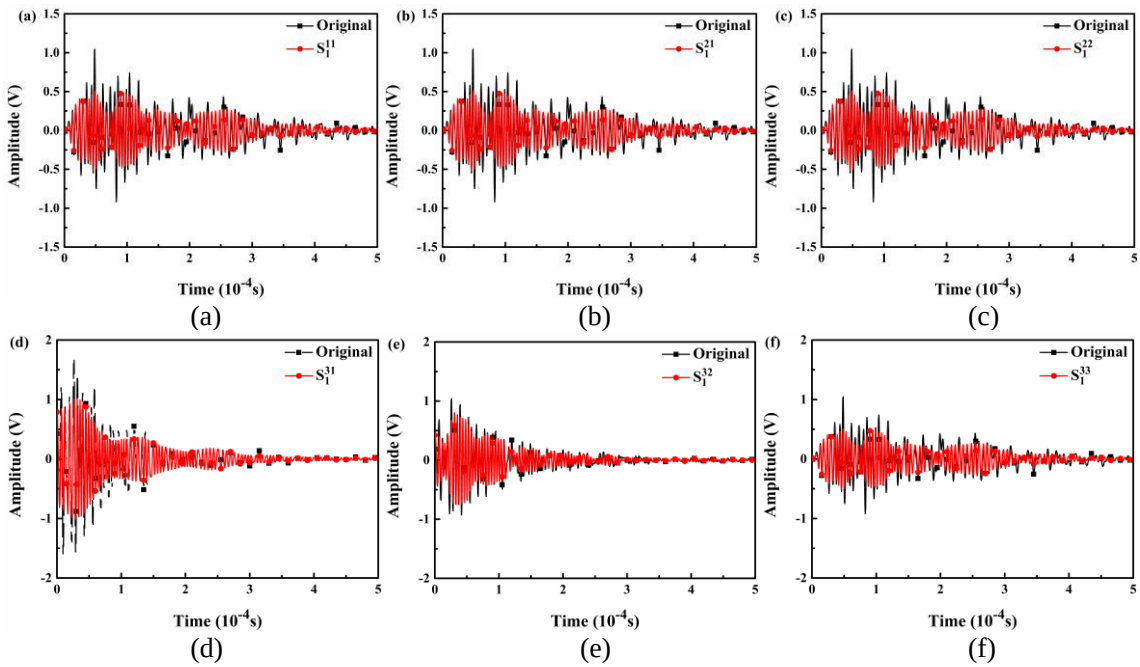

Figure 5: Time presentations of the original AE signal and its first IMF captured from the fiber multi-stage fracture of single fiber pull-out process: (a) single stage, (b) process 1 and (c) process 2 in double stage, (d) process 1, (e) process 2 and (f) process 3 in triple stage.

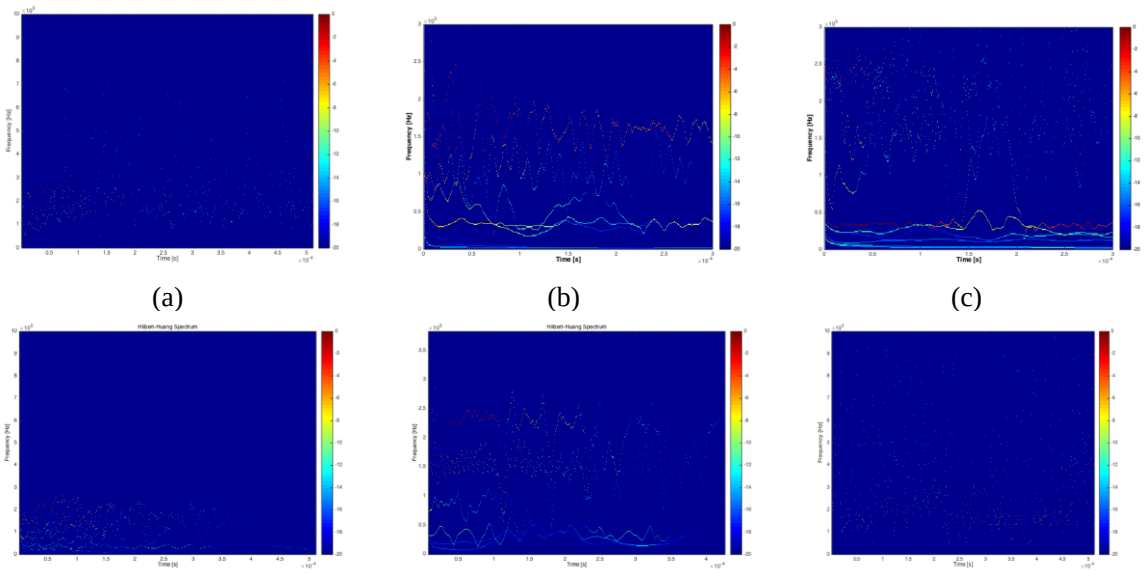

(a) (b) (c)

(d) (e) (f)

Figure 6: Hilbert-Huang transform spectra of the AE signals (a) in Figure 5 (a), (b) in Figure 5 (b), (c) in Figure 5 (c), (d) in Figure 5 (d), (e) in Figure 5 (e) and (f) in Figure 5 (f)

4.2 Statistical analysis on the multi-stage fracture performance of SFRCs

Figure 7 (a) shows the distributions of the number of occurrences of single, double and triple stage fracture of the SFRCs recorded via Weibull statistical analysis method and the corresponding Weibull distribution was illustrated in Figure 7 (b). The effects of the multi-layer interfaces on the interfacial failure behaviors and the pullout performances of SFRCs were depicted. It can be seen that double and triple stage fracture were main failure modes due to the distinct structure of multi-layer interfaces.

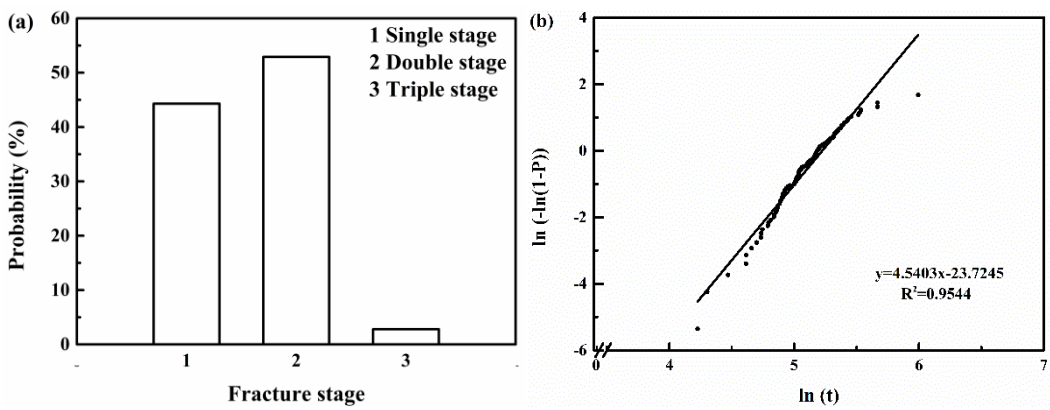

Figure 7: (a) Distribution of the number of occurrences of multi-stage of the SFRCs and (b) corresponding Weibull distribution.

4.3 Comparisons of the applied stress on sisal fiber with multi-layer interface between experiments and theories

The experimental applied stresses versus displacement for SFRCs with different embedded fiber lengths were plotted. Based on the numerical results, the theoretical applied stresses at different stages (see Figure 8) with various embedded fiber lengths were solved. A multi-stage failure mode of PFRC subject to tensile load was clearly presented, which was produced by the sequential fracture of the three interfaces. To conclude, theoretical analysis was consistent with the experimental applied stress in the pull-out tests. The morphologies of fracture surfaces of the sisal fibers after the pull-out tests obtained by SEM further prove the validity of the present double interface model in predicting the

fracture behavior of PFRC subject to tensile load. Therefore, the existence of the multi-layer structure of the sisal fiber leads to multiple interfacial failure modes of SFRCs in the pull-out tests. The accuracy of the double interface was also compared to that of traditional single interface model in terms of predicting multi-stage fracture behavior of SFRC. As shown in Figure 9, the accuracy of the multiple (double and triple) interface was also compared to that of traditional single interface model in terms of predicting multi-stage fracture behavior of SFRC. It could be seen that the results calculated by the double and triple interface model was more consistent with the experimental ones than those by the single interface model, which indicated that the double and triple interface model developed in the current work was more appropriate to reveal the multi-scale and multi-layer interfacial damage mechanism of PFRCs.

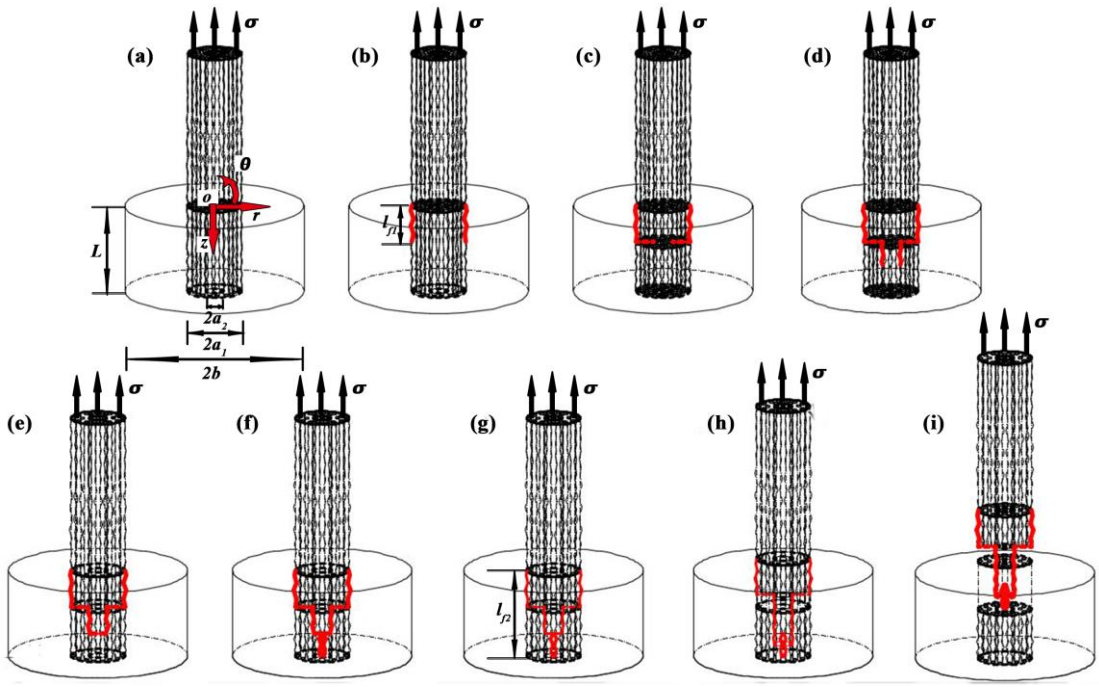

Figure 8: Schematic of the three-interface model describing multi-stage fracture and pull-out behaviors of SFRCs: (a) original model, (b) and (c) process 1, (d) and (e) process 2, (f) and (g) process 3, (h) and (i) pull-out process.

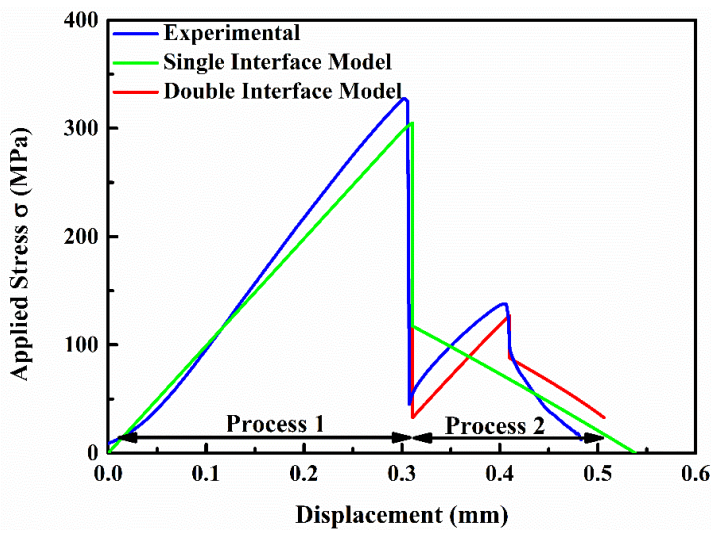

Figure 9: Comparison of the applied stress between experiment, single, double and triple interface model. ($L = 0.332mm$ is used for this figure)

4.4 Stress distributions during the debond process of SFRCs simulated by FEM

The stress distributions on the interfaces were obtained by simulating the single sisal pullout process. As shown in Figure 10, the interface occurred partial debonding firstly and totally debonding happened. The debond length could be ascertained by the present finite element analysis. The influence of different embedded length on the interfacial failure behaviors and the interface properties will be investigated in our next work.

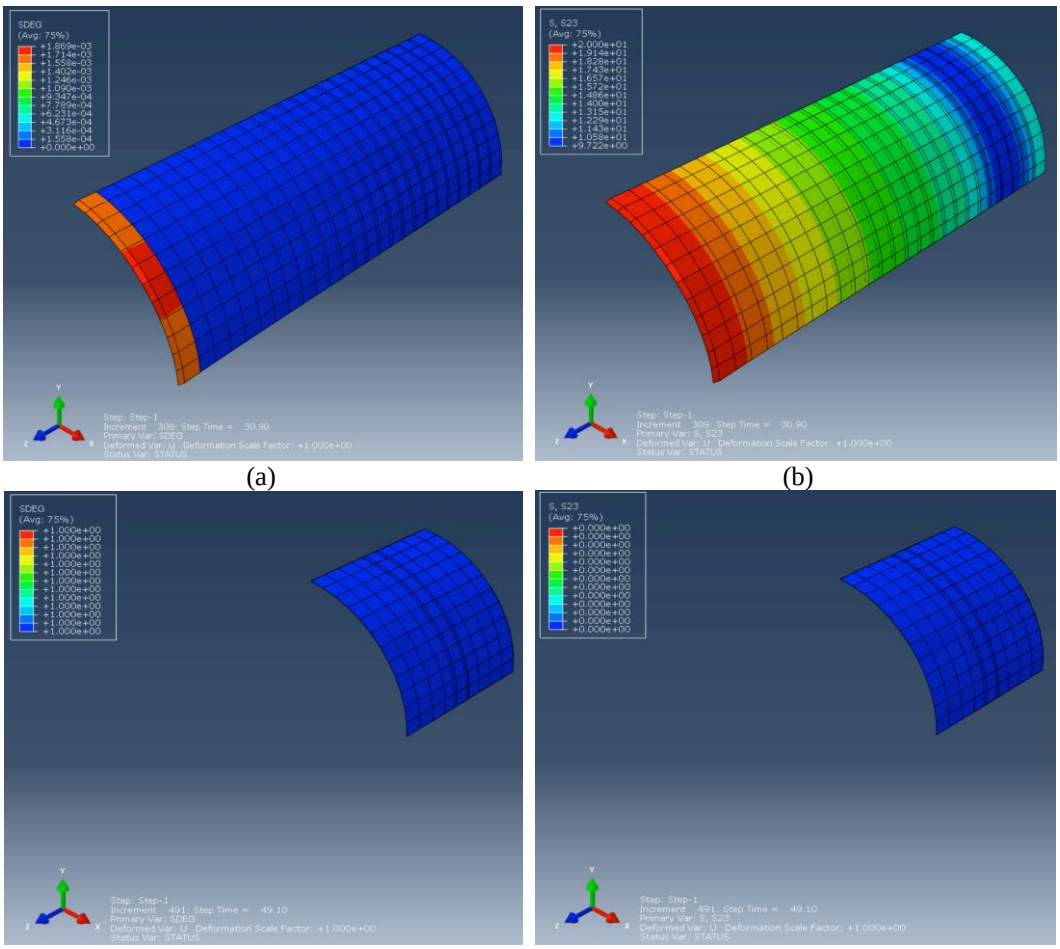

Figure 10: Contour of the three-interface model describing multi-stage fracture and pull-out behaviors of SFRCs: (a) interface damage factor, (b) interface stress at the beginning of debond, (c) interface damage factor and (d) interface stress at the end of debond.

5 CONCLUSIONS

The interfacial failure behaviors of SFRCs were investigated experimentally and theoretically in the current study. The multi-scale and multi-layer structure of the sisal fibers made the interfacial failure mechanisms in their reinforcing composites different with those of traditional artificial fiber reinforced composites. The unique multi-stage interfacial failure behaviors of SFRCs were obtained and characterized based on AE events recorded in the single fiber pull-out experiments. The residual pullout strength of SFRC was found to be reduced gradually when subject to tensile load. With the use of the proposed double and three-interface model, the multi-interfacial failure process and mechanisms of SFRCs in the pull-out tests were further revealed and accounted for. To sum up, the existence of multi-interfaces of PFRCs and the differences of their interfacial properties introduce the multi-scale and multi-layer failure behaviors of PFRCs.

ACKNOWLEDGEMENTS

This paper was supported by Shanghai Outstanding Academic Leaders Plan (16XD1402900) and the Fundamental Research Funds for the Central Universities.

REFERENCES

[1] F.D. Silva, N. Chawla and R.D. de Toledo. Tensile behavior of high performance natural (sisal) fibers. *Composites Science and Technology*, **68**, 2008, pp. 3438-3443.
[2] C. Elanchezhian, B.V. Ramnath, G. Ramakrishnan, M. Rajendrakumar, V. Naveenkumar and M.K. Saravanakumar. Review on mechanical properties of natural fiber composites. 2016, pp.
[3] M.P.M. Dicker, P.F. Duckworth, A.B. Baker, G. Francois, M.K. Hazzard and P.M. Weaver. Green composites: A review of material attributes and complementary applications. *Composites Part A: Applied Science and Manufacturing*, **56**, 2014, pp. 280-289.
[4] Y. Li, Y. Luo and S. Han. Multi-scale structures of natural fibres and their applications in making automobile parts. *Journal of Biobased Materials and Bioenergy*, **4**, 2010, pp. 164-171.
[5] Y. Li, S.M. Cai and X.L. Huang. Multi-scaled enhancement of damping property for carbon fiber reinforced composites. *Composites Science and Technology*, **143**, 2017, pp. 89-97.
[6] H. Mamtaz, M.H. Fouladi, M. Al-Atabi and S. Narayana Namasivayam. Acoustic absorption of natural fiber composites. *Journal of Engineering*, **2016**, 2016, pp.
[7] X.H. Sui, J. Shi, H.W. Yao, Z.W. Xu, L. Chen, X.J. Li, M.J. Ma, L.Y. Kuang, H.J. Fu and H. Deng. Interfacial and fatigue-resistant synergetic enhancement of carbon fiber/epoxy hierarchical composites via an electrophoresis deposited carbon nanotube-toughened transition layer. *Composites Part a-Applied Science and Manufacturing*, **92**, 2017, pp. 134-144.
[8] M. Alimardani, M. Razzaghi-Kashani and M.H.R. Ghoreishy. Prediction of mechanical and fracture properties of rubber composites by microstructural modeling of polymer-filler interfacial effects. *Materials & Design*, **115**, 2017, pp. 348-354.
[9] Z.B. Zhao, K.Y. Teng, N. Li, X.J. Li, Z.W. Xu, L. Chen, J.R. Niu, H.J. Fu, L.H. Zhao and Y. Liu. Mechanical, thermal and interfacial performances of carbon fiber reinforced composites flavored by carbon nanotube in matrix/interface. *Composite Structures*, **159**, 2017, pp. 761-772.
[10] E.O. Ogunsona, M. Misra and A.K. Mohanty. Impact of interfacial adhesion on the microstructure and property variations of biocarbons reinforced nylon 6 biocomposites. *Composites Part A: Applied Science and Manufacturing*, **98**, 2017, pp. 32-44.
[11] K. Tanaka, K. Minoshima, W. Grela and K. Komai. Characterization of the aramid/epoxy interfacial properties by means of pull-out test and influence of water absorption. *Composites Science and Technology*, **62**, 2002, pp. 2169-2177.
[12] L.M. Zhou, Y.W. Mai and L. Ye. Analyses of Fiber Push-out Test Based on the Fracture-Mechanics Approach. *Composites Engineering*, **5**, 1995, pp. 1199-1219.
[13] J.M. Park, J.W. Kong, J.W. Kim and D.J. Yoon. Interfacial evaluation of electrodeposited single carbon fiber/epoxy composites by fiber fracture source location using fragmentation test and acoustic emission. *Composites Science and Technology*, **64**, 2004, pp. 983-999.
[14] J.M. Park, W.G. Shin and D.J. Yoon. A study of interfacial aspects of epoxy-based composites reinforced with dual basalt and SiC fibres by means of the fragmentation and acoustic emission techniques. *Composites Science and Technology*, **59**, 1999, pp. 355-370.
[15] T. Suzuki, M. Sato and M. Sakai. Fiber pullout processes and mechanisms of a carbon fiber reinforced silicon nitride ceramic composite. *Journal of Materials Research*, **7**, 1992, pp. 2869-2875.
[16] M. Sakai, R. Matsuyama and T. Miyajima. The pull-out and failure of a fiber bundle in a carbon fiber reinforced carbon matrix composite. *Carbon*, **38**, 2000, pp. 2123-2131.
[17] C. Marotzke. Influence of the fiber length on the stress transfer from glass and carbon fibers into a thermoplastic matrix in the pull-out test. *Composite Interfaces*, **1**, 1993, pp. 153-166.
[18] M. Manoharan, A. Sharma, A. Desai, M. Haque, C. Bakis and K. Wang. The interfacial strength of carbon nanofiber epoxy composite using single fiber pullout experiments. *Nanotechnology*, **20**, 2009, pp. 295701.

[19] L.M. Zhou, J.K. Kim and Y.W. Mai. Interfacial debonding and fiber pull-out stresses .2. A new model based on the fracture-mechanics approach. *Journal of Materials Science*, **27**, 1992, pp. 3155-3166.
[20] L.M. Zhou, Y.W. Mai and C. Baillie. Interfacial debonding and fiber pull-out stresses .5. A methodology for evaluation of interfacial properties. *Journal of Materials Science*, **29**, 1994, pp. 5541-5550.
[21] H.Y. Liu, L.M. Zhou and Y.W. Mai. On fiber pull-out with a rough interface. *Philosophical Magazine a-Physics of Condensed Matter Structure Defects and Mechanical Properties*, **70**, 1994, pp. 359-372.
[22] J.H. Tsai, A. Patra and R. Wetherhold. Finite element simulation of shaped ductile fiber pullout using a mixed cohesive zone/friction interface model. *Composites Part a-Applied Science and Manufacturing*, **36**, 2005, pp. 827-838.
[23] X.Y. Chen, I.J. Beyerlein and L.C. Brinson. Curved-fiber pull-out model for nanocomposites. Part 2: Interfacial debonding and sliding. *Mechanics of Materials*, **41**, 2009, pp. 293-307.
[24] Y.Y. Jia, W.Y. Yan and H.Y. Liu. Carbon fibre pullout under the influence of residual thermal stresses in polymer matrix composites. *Computational Materials Science*, **62**, 2012, pp. 79-86.
[25] Y. Li, H. Ma, Y.O. Shen, Q. Li and Z.Y. Zheng. Effects of resin inside fiber lumen on the mechanical properties of sisal fiber reinforced composites. *Composites Science and Technology*, **108**, 2015, pp. 32-40.
[26] M. Aslan. Investigation of damage mechanism of flax fibre LPET commingled composites by acoustic emission. *Composites Part B-Engineering*, **54**, 2013, pp. 289-297.
[27] Y. Li, Y.W. Mai and L. Ye. Sisal fibre and its composites: a review of recent developments. *Composites Science and Technology*, **60**, 2000, pp. 2037-2055.
[28] R.H. Newman, M.J. Le Guen, M.A. Battley and J.E.P. Carpenter. Failure mechanisms in composites reinforced with unidirectional Phormium leaf fibre. *Composites Part a-Applied Science and Manufacturing*, **41**, 2010, pp. 353-359.
[29] A.C.N. Singleton, C.A. Baillie, P.W.R. Beaumont and T. Peijs. On the mechanical properties, deformation and fracture of a natural fibre/recycled polymer composite. *Composites Part B-Engineering*, **34**, 2003, pp. 519-526.
[30] N.E. Huang, Z. Shen, S.R. Long, M.C. Wu, H.H. Shih, Q. Zheng, N.C. Yen, C.C. Tung and H.H. Liu. The empirical mode decomposition and the Hilbert spectrum for nonlinear and non-stationary time series analysis. *in: Proceedings of the Royal Society of London A: Mathematical, Physical and Engineering Sciences*, The Royal Society, 1998, pp. 903-995.